Chemical Engineering Science 280 (2023) 118992

Contents lists available at ScienceDirect

Chemical Engineering Science

journal homepage: www.elsevier.com/locate/ces

Can fluid-solid contact area quantify wettability during flow? – A parametric study

Deepshikha Singh [a], Shantanu Roy [a], Harish Jagat Pant [b], Jyoti Phirani [c,*]

[a] Department of Chemical Engineering, Indian Institute of Technology Delhi, Hauz Khas, New Delhi, India
[b] Isotope and Radiation Application Division, Bhabha Atomic Research Centre, Trombay, Mumbai, India
[c] Department of Civil and Environmental Engineering, University of Strathclyde, Glasgow, United Kingdom

ARTICLE INFO

Keywords:
Two-tracer method
Wettability
Liquid-solid interfacial area
Grain size
Surface roughness

ABSTRACT

Wettability characterisation in a porous medium is challenging owing to the heterogeneity and large-scale of the interacting surface. Measuring the liquid-solid contact area can be used as a real-time wettability quantification at the Darcy scale. However, flow, grain size, and saturation path can affect the liquid-solid contact area. In this work, we use the two-tracer experiments to quantify the liquid-solid contact area and relate it with different parameters affecting the liquid-solid contact area. We do experiments at different conditions, i.e. (a) when the organic phase is at residual saturation and (b) when both phases flow. When the organic phase is immobile, increasing the flow rate does not change the residual saturation significantly; however, the water-solid contact area increases because of the increased corner flow. When both organic and aqueous phases flow, the relationship between the water saturation and water-solid contact area is found to be dependent on the grain size.

1. Introduction

Wettability characterisation in a porous medium is challenging due to the petrophysical variations in the properties of the porous medium, heterogeneity of the surface, unavailability of the pores for visual inspection and the inability of micro-scale imaging for large-scale. Wettability strongly affects the fluid flow dynamics by controlling the capillary pressure in a porous medium during multiphase flow. Wettability plays a vital role in many natural and industrial applications, such as groundwater remediation (Huling and Weaver, 1991), enhanced oil recovery (EOR) (Ju et al., 2012), wicks of a loop heat pipe (Nemec, 2017; Li et al., 2019; Ashraf et al., 2023), high-performance lithium-ion batteries (Jeon, 2019), CO_2 sequestration (Farokhpoor et al., 2013), particle coating (Woudt, 1959), printing techniques (Tian et al., 2013), catalyst behaviour in packed bed reactors (Singhal and Dranchuk, 1975), textile industry, paper microfluidic devices (Akyazi et al., 2018) and membrane distillation (Yao et al., 2020). Therefore, wettability quantification of a porous medium is important for designing fluid flow strategies in natural porous mediums such as geological reservoirs or designing a porous medium for lithium-ion batteries.

A lot of literature is available for quantifying wettability in porous geological reservoirs (Anderson, 1986a, 1986b, 1986c, 1987a, 1987b, 1987c; Rücker et al., 2020; Armstrong et al., 2019; Jain et al., 2003; Strand et al., 2006; Standnes and Austad, 2003, 2000). Quantifying wettability using contact angle is limiting due to the scale and heterogeneity of the porous medium (Armstrong et al., 2016; Liu et al., 2017; McClure et al., 2016; Armstrong et al., 2021). Wettability quantification at the Darcy scale still needs to be fully understood because of the surface roughness and multiphase fluid flow (Golparvar et al., 2018; Lin et al., 2019; Brusseau et al., 2010; Araújo and Brusseau, 2019). High-resolution imaging techniques such as X-ray micro-CT and electron microscopy have been used to measure fluid-solid and fluid-fluid contact areas that can quantify wettability during the multiphase flow (Joekar-Niasar et al., 2008; Joekar-Niasar and Hassanizadeh, 2012; McClure et al., 2018; Garfi et al., 2020; Herring et al., 2021). However, applying these techniques at a large-scale and especially in geological reservoirs is challenging because of the high resolution and inaccessibility of the geological reservoirs for imaging at the required scale (Schnaar and Brusseau, 2005; Brusseau et al., 2007; Russo et al., 2009; Brusseau et al., 2009; Christensen and Tanino, 2017; Tabar et al., 2020).

In our previous work, we took a first step to measure the liquid-solid interfacial area using tracers in flowing conditions that can differentiate between the different wetting conditions (Singh et al., 2021, 2022). Previous studies show that the wetting phase had 10% more contact area with the porous solid at the same residual saturation than the non-wetting phase (Singh et al., 2021). Further, we demonstrated exper-

* Corresponding author.
E-mail address: jyoti.phirani@strath.ac.uk (J. Phirani).

https://doi.org/10.1016/j.ces.2023.118992
Received 12 April 2023; Received in revised form 9 June 2023; Accepted 11 June 2023
Available online 16 June 2023

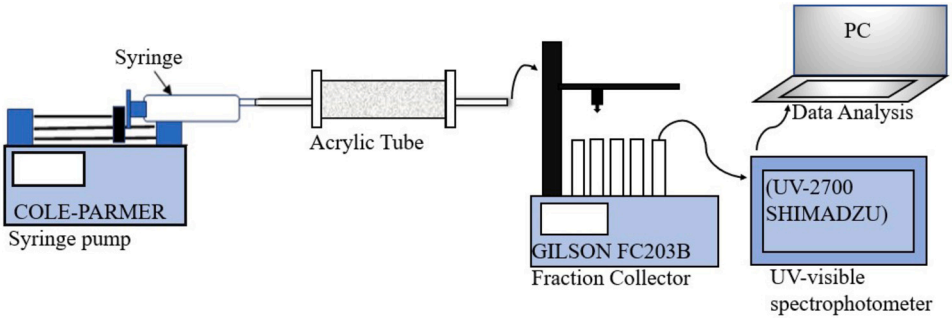

Fig. 1. Schematic of flow experimental setup.

imentally that the wetting conditions of the porous medium also alter the liquid-solid contact area in addition to liquid saturations. Therefore, the liquid-solid contact area is found to be dependent on two parameters: the wettability of the solid and the liquid saturation.

In immiscible two-phase flows, fluid saturations and their distribution in immiscible two-phase flows are influenced by the distribution of particle sizes, flow velocity, gravity, flow process to reach a saturation (i.e. injection process of initially injecting with water or with oil in this study), and surface morphology of the grains. Generally, wetting fluid occupies the surfaces and smaller pores, while non-wetting fluids accumulate in the central part of the bigger pores (Alhosani et al., 2021). To understand how these parameters will affect the liquid-solid contact area, a parametric study is required. We used our two-tracer technique to further develop the method for quantifying wettability.

In this work, we use the two-tracer method in an artificial porous medium to quantify the liquid-solid contact area. We explore how grain size, gravity, surface morphology, and flow processes i.e. the injection process of initially injecting with water or oil, affect the liquid-solid contact area. We perform experiments at different flow rates and conditions to see the impact on the liquid-solid contact area. In the end, we show that when we have an immobile non-wetting phase, the flow rate does not change the residual liquid saturation significantly, but the water-solid contact area increases with the increasing flow rate of the water. We also show that when oil and water flow together in the water-wet porous medium, the water saturation and water-solid contact area increase with an increasing flow rate of water.

The paper is organised as follows. Section 2 describes the method/theory and materials used in the experimental setup. In Section 3, we report the results of multiphase flow experiments and further discuss the effects of different parameters on measured water-solid contact area. A summary and conclusion follow in Section 4.

2. Methods and materials

2.1. Experimental setup

Fig. 1 shows a schematic of the experimental setup. We pack the glass beads or sand in an acrylic cylindrical tube of length = 15 cm and diameter = 2 cm to make a proxy porous medium. While filling the beads or sand in the cylinder, we intermittently tap the cylinder for uniform and dense packing. We use Whatman filter paper on both ends of the tube to prevent the migration of the particles in the injection and production pipelines. We use a syringe pump to inject the water or oil into the packed porous medium. In a fraction collector, we collect the exit stream in the tubes at pre-specified time intervals. We use a UV-visible spectrophotometer (UV-2700 SHIMADZU) to analyse the tracer concentrations in the effluent samples (Singh et al., 2021, 2022).

2.2. Tracer test theory

In a tracer test, the first moment of the normalised effluent tracer concentration with time equals the mean residence time (MRT) of the tracer for a pulse input of an ideal tracer. For a step input, the mean residence time is related to the effluent tracer concentration as given in the Eqn. (1). The mean residence time can also be calculated using the process parameters, i.e. fluid volume inside the porous medium and the flow rate. Schwartz et al. (1976) related the mean residence time of an adsorbing tracer with the effluent tracer concentration with the time curve and the process parameters as given in Eqn. (2).

$$\left[\int_0^\infty \left(1-\frac{C_{exit}(t)}{C_T}\right) dt\right]_{experimental} = \tau_i = \left[\frac{\phi V}{Q}\right]_{theoretical} \tag{1}$$

$$\left[\int_0^\infty \left(1-\frac{C_{exit}(t)}{C_T}\right) dt\right]_{experimental} = \tau_a = \left[\frac{\phi V}{Q} + \frac{K_a A_T}{Q}\right]_{theoretical} \tag{2}$$

where $C_{exit}(t)$ is the exit tracer concentration at time t after the start of the tracer injection and C_T is the initial tracer concentrations (g/l), τ_i is the MRT of the ideal tracer (min) and τ_a is the MRT of the adsorbing tracer (min), ϕ is the porosity, V is the bulk volume of the porous medium (ml), Q is the liquid injection rate (ml/min), K_a is the adsorption partition coefficient onto the solid matrix (ml/g), and A_T is the total mass of the glass beads or sand in contact with the water (g), or total water wetted solid contact area (m^2). For the applicability of Eqn. (2), there are some assumptions, which are explained in our previous publication (Singh et al., 2022). If we inject an ideal tracer and an adsorbing tracer in the porous medium, then using the exit concentration, we can find the MRTs using Eqns. (1), (2). The difference of the two MRTs is equal to $\frac{K_a A_T}{Q}$, therefore to find the contact area of the fluid with the porous solid A_T we should know the flow rate Q and adsorption coefficient K_a. This equation can be used during multiphase flow to find the A_T of a particular fluid in contact with the porous solid. Therefore, now we find the K_a of the adsorbing tracers we have used.

2.3. Methodology to estimate K_a of the adsorbing tracer

We use single-phase flow experiments and Eqn. (1) and (2) to estimate the K_a of the adsorbing tracer in our system. First, we measure the porous medium's porosity and pore volume using the weight of the liquid trapped in the pores (Singh et al., 2022). After that, we perform a water-tracer flow experiment in the packed horizontal tube. We inject the ideal tracer as a step input at a particular flow rate until the exit tracer concentration equals the injected tracer concentration. To change the water flow to tracer dissolved water flow, we stopped the syringe pumps for a few seconds and change the syringe of water with the water-tracer syringe. To minimise air entrapment, we ensure that the syringe and the tube are fully filled with liquids during the change. To remove the tracer from the packing, we inject five pore volumes of deionised water so that the UV-vis spectrum of the tracer is not visible in the effluent. Then, we perform the water-tracer flow experiment with the adsorbing tracer at the same flow rate and conditions. We collect the effluent tracer at regular intervals to construct an exit tracer concentration profile with time. Using the concentration profiles of the adsorbing

Table 1
Estimated K_a for the adsorbing tracer (V = 47.10 ml).

Size of the beads	Q, $\frac{ml}{min}$	ϕ	$\tau_i = \phi V/Q$, min	A_T, g	$\tau_i = \int_0^\infty [1 - \frac{C_{exit}(t)}{C_T}]dt$, min (FSS)	$\tau_a = \int_0^\infty [1 - \frac{C_{exit}(t)}{C_T}]dt$, min (STS)	$(\tau_a - \tau_i)\frac{Q}{A_T} = K_a$, $\frac{ml}{g}$
0.15-0.2 mm	0.25	0.41	77.24	78.91	78.76 ± 0.48	87.13 ± 0.79	**0.027**
	0.50	0.41	38.62	78.91	40.23 ± 0.76	44.88 ± 0.60	**0.029**
	1.00	0.41	19.31	78.91	19.45 ± 0.36	21.80 ± 0.50	**0.030**
2 mm	0.25	0.42	79.13	78.80	79.22 ± 0.74	88.76 ± 0.20	**0.030**
	0.50	0.42	39.56	78.80	41.03 ± 0.07	45.98 ± 0.16	**0.031**
	1.00	0.42	19.78	78.80	20.23 ± 0.24	22.76 ± 0.07	**0.032**

Table 2
The estimated water-solid contact area of the cleaned glass beads (A_w) at various residual oil saturation at different flow rates and different bead sizes (V = 47.10 ml, K_a = 0.03, ml/g).

Bead size	Flow rate (Q), $\frac{ml}{min}$	A_T, g	S_{wc}, (MB)	S_w (MB)	τ_i' (FSS), min	τ_a' (STS), min	$S_w = \frac{\tau_a}{\tau_i}$	$A_w = (\tau_a' - \tau_i')\frac{Q}{K_a}$, g	$\frac{A_w}{A_T}$
0.15-0.2 mm	0.25	78.91	0.26	0.83	65.37 ± 0.22	73.14 ± 0.21	0.83	64.75	0.82
	0.50	78.91	–	0.84	34.20 ± 0.25	38.60 ± 0.23	0.85	73.33	0.93
	1.00	78.91	–	0.85	16.73 ± 0.32	19.02 ± 0.22	0.86	76.33	0.97
2 mm	0.25	78.80	0.25	0.71	57.04 ± 0.32	61.96 ± 0.41	0.72	41.00	0.52
	0.50	78.80	–	0.72	29.95 ± 0.35	33.21 ± 0.32	0.73	54.33	0.69
	1.00	78.80	–	0.75	14.97 ± 0.32	16.81 ± 0.32	0.74	61.33	0.78

and ideal tracers, we find their respective MRTs (MRT graphs for each of the tracers are given in supplementary material). The difference in MRTs is equal to $\frac{K_a A_T}{Q}$. During the single-phase flow experiments, A_T is the total mass or surface area of the solids (sand or beads) present in the porous system and hence is known. Using the flow rate and the known A_T, we estimate the K_a of the adsorbing tracer in our system. We repeat the tracer injection experiment three times at one particular flow rate in the same packing of the porous medium for repeatability. We also repeat the experiment at a different flow rate to demonstrate that K_a is independent of the flow rate.

Because K_a is an isothermal property, it will be constant for the same liquid and solid pair during the multiphase flow. Therefore, using the estimated K_a, we can measure the water-solid contact area at different flow conditions and saturations during the multiphase flow.

The multiphase flow methodology used is dependent on the parameter being tested. Therefore, the multiphase flow procedure is in the results section.

2.4. Materials

In this study, we use N-dodecane as the organic phase and Deionised Water as an aqueous phase. As our proxy porous medium, we use glass beads pack and a sand pack in a cylindrical acrylic tube. We clean the glass beads with 0.1 M HCl solution before packing to make them water wet. After this, we wash the glass beads with distilled water to remove the residues and dry them in an oven at 80 °C till they are dehydrated (Singh et al., 2022). We use quartz sand (average grain diameter 0.2 mm) in its original state. We have purchased glass beads and sand from GLR innovators in New Delhi, India. We use Fluorescein Sodium Salt (FSS), $C_{20}H_{10}Na_2O_5$ (376.28 g/mol, 1.6 g/ml) and Sodium Thiosulfate (STS), $Na_2S_2O_3.5H_2O$ (248.18 g/mol, 1.67 g/ml) as ideal and adsorbing aqueous phase tracers, respectively. We use Trans-Stilbene (TSB), $C_{14}H_{12}$ (180.25 g/mol, 0.97 g/ml) and Oil Red O, $C_{26}H_{24}N_4O$ (408.49 g/mol) as ideal and adsorbing organic phase tracers, respectively. All chemicals are purchased from Sigma-Aldrich Chemicals Pvt Ltd., India.

We will now show how the liquid-solid contact area varies with flow rate, grain size, gravity effects, roughness, and flow process, i.e. the process used to reach a particular state of saturation and flow conditions.

3. Results

3.1. Effect of grain size on measured water-solid contact area

Grain size controls the pore size and, consequently, affects the capillary forces, viscous forces and the solid surface area per unit weight or volume of the grains in a porous medium (Cai and Yu, 2010). To understand the effect of the grain size on the liquid-solid interfacial area, we use cleaned glass beads of diameters 0.15-0.2 mm and 2 mm to create two separate proxy porous media using the acrylic cylindrical tube. We prepare the porous medium for multiphase flow experiments by injecting water and oil sequentially in the glass beads packing.

3.1.1. Preparation of the porous medium for multiphase flow

To prepare the porous medium for the tracer injection, we first inject the water at a rate of 1 ml/min in the porous system from the bottom while the tube is oriented vertically. This is to avoid any instabilities during water injection. We find the porosity by weighing the empty and water-filled porous medium. The porosity of the 0.15-0.2 mm beads is 0.41 ± 0.01, and for 2 mm beads is 0.42 ± 0.01. We then estimate the K_a of the water tracers while the cylindrical packing orientation is horizontal and using the methodology described in Section 2.3. In Table 1, we show the MRT estimated using the exit tracer concentration profile in Column 6. The measured MRT shows an excellent match with the MRT calculated using the process parameters shown in column 4 in the table. This confirms that our tracer experiments are performing as expected. As is evident from Table 1, we perform the single-phase flow experiments at three different flow rates, 0.25, 0.5, and 1 ml/min, to estimate the K_a of the adsorbing water tracer. The average estimated K_a using Eqns. (1) and (2) for 2 mm and 0.15 – 0.2 mm glass beads are 0.03 ±0.001 and 0.03 ±0.002 (ml/g), respectively, as shown in Table 1.

After completing the single-phase flow experiments, we inject oil at a flow rate of 1 ml/min to reach the maximum oil saturation. For oil reservoirs, this will mimic the initial condition of the reservoirs (Chen et al., 2018). At this point, the water saturation in the two packings is measured by mass balance given in column 4 of Table 2. Once we reach a steady state, i.e., the exit stream has only oil and the water is immobile, then we displace oil with water during the secondary imbibition process.

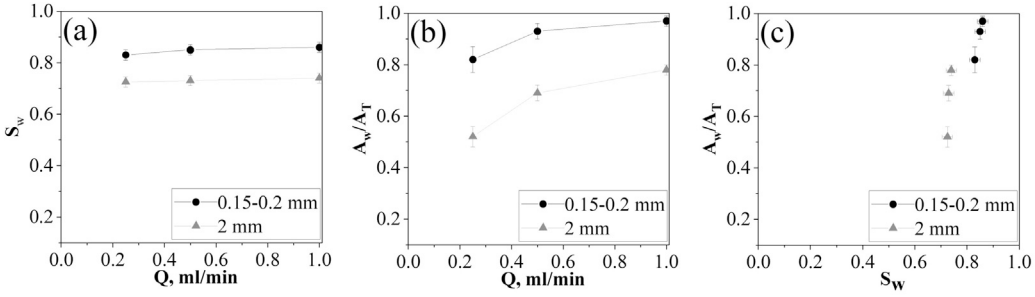

Fig. 2. The effect of grain size on (a) water saturation, (b) the fractional water-solid contact area; at different water injection rates, and (c) the fractional water-solid contact area as a function of the water saturation at different water injection rates, when water is in the mobile phase, and oil is in the residual phase.

3.1.2. Estimation of water-solid contact area at residual oil saturation

We first inject water during secondary displacement at a flow rate of 0.25 ml/min. We use the material balance (MB) to calculate the displaced oil, which is 73% for 2 mm beads packing and 83% for 0.15-0.2 mm beads packing. Once we reach a steady state for the secondary imbibition and oil is immobile, i.e. at the residual saturation, the exit stream has only water. Then we follow the procedures described above in Section 2.3 to perform the water tracer flow experiments. We calculate the MRTs using the exit concentration profile of the tracer at the residual oil saturation using Eqn. (3) and (4) for the ideal and the adsorbing tracers, respectively.

$$\int_0^\infty \left(1-\frac{C_{exit}(t)}{C_T}\right)_{experimental} dt = \tau_i' = \left(\frac{\phi V S_i}{Q}\right)_{theoretical} \tag{3}$$

$$\int_0^\infty \left(1-\frac{C_{exit}(t)}{C_T}\right)_{experimental} dt = \tau_a' = \left(\frac{\phi V S_i}{Q}+\frac{K_a A_w}{Q}\right)_{theoretical} \tag{4}$$

where $C_{exit}(t)$ is the exit tracer concentration at time t after the start of the tracer injection and C_T is the initial tracer concentrations (g/l), τ_i' is the MRT of the ideal tracer (min) and τ_a' represents the MRT of the adsorbing tracer (min). S_i represents the mobile-phase i.e. water saturation and A_w represents the water-solid contact area (g).

Eqns. (3) and (4) are similar to Eqns. (1) and (2). However, if we have multiple phases in the porous systems, we need to include the flowing phase's saturation in our equations for the volume of the phase in the porous system. This allows us to validate our multiphase flow tracer experiments by comparing water saturation estimated by material balance (MB) and calculated using Eqns. (1) and (3). We show these results in Table 2 in columns 5 and 8 and see a good match in the saturations. We calculate the water-solid contact area in the porous medium (A_w) while water is the mobile phase using Eqns. (3) and (4) and use three repetitions of the water tracer experiments at the water flow rate of 0.25 ml/min as shown in column 9 of Table 2. We now increase the water flow rate to 0.5 ml/min. As the flow rate increases, we get some extra oil from the glass bead packing. Therefore, we measure the new residual oil saturation at a 0.5 ml/min water flow rate. We perform three sets of water tracer experiments at a 0.5 ml/min water flow rate and then increase the water injection rate to 1 ml/min. We again measure the new residual oil saturation at a 1 ml/min water flow rate. We then complete three tracer experiments at a water injection rate of 1 ml/min. Hence, for consistency in all the experiments, we used the same packing of the glass beads. From Table 2 and Fig. 2 (a), we find that the additional oil displacement is negligible at higher water injection rates, especially for a 2 mm beads packing. Furthermore, we also observe that the additional oil displacement has not changed much for the 0.2 mm beads packing either. However, we have obtained 10% higher oil recovery from the 0.2 mm beads packing than the 2 mm beads packing by the material balance. This is because, in the water-wet porous medium, water prefers the smaller pores and pore boundaries due to capillary forces, disconnecting the oil droplets or ganglia in the central part of larger pore spaces, which become immobile, resulting in residual oil saturation. For the larger pores in 2 mm beads, the oil ganglia or droplet sizes in the pores are large (Cense and Berg, 2009). We need to provide an additional viscous force by increasing the water injection rate to overcome the capillary force and mobilise the oil droplet or ganglia through the pore body to change the saturation. Considering the capillary number (C_a) (Günther and Jensen, 2006) given below

$$C_a = \frac{\mu_w u}{\sigma} \times \frac{\mu_w}{\mu_o} \tag{5}$$

where μ_w and μ_o are the viscosity of water and oil, respectively, in Pa.s, and u is the average inlet water injection velocity in m/s. For the multiphase fluid flow in a porous medium, the interstitial velocity in the pores u is related to the Darcy velocity U via $u = U/\phi S_w$.

Using Eqn. (5), the capillary number is of the order of 10^{-7} which does not change significantly when we change water injection rate 0.25 ml/min, i.e. 3.9×10^{-5} m/s to 1 ml/min. We use the viscosity of the water 1×10^{-3} Pa.s, and interfacial tension 0.034 N/m. For mobilisation of the oil droplet in the water-wet porous medium, capillary numbers should be in the orders of magnitude 10^{-3} or higher (Cense and Berg, 2009). Therefore, we do not get a significant change in saturations as shown in Fig. 2 (a).

Further, we show experimental results in Fig. 2 (b), which shows that there is a sharp change in the water-solid contact area with flow rates. This is due to the significant corner flow phenomena (Zhao et al., 2016), in which, at low capillary numbers, water advances by coating the perimeters of the solid surface rather than by filling the pore bodies. At a low flow rate, there can be more oil present in contact with the solid surface, and when we increase the flow rate, the water flow path changes to coat more surface of the glass beads. The water-solid contact area increases with no significant change in the water saturation, as shown in Fig. 2 (c). This is due to the corner flow phenomenon. We also note from Fig. 2 (b) and (c) that the 2 mm glass beads have less water-solid contact area and water saturation than 0.15-0.2 mm glass beads at the same water injection rate, which means that bead size affects the water-solid contact area and the saturation.

3.1.3. Estimation of water-solid contact area with two flowing phases

Further, we use the same setup to perform the two-phase flow experiments where aqueous and organic phases flow simultaneously in the porous medium. Using this method, we change the water saturation by the design of the experiment. The previous experiment ended when a water tracer was injected at a flow rate of 1 ml/min. We again flush the water tracer out from the porous medium by injecting several pore volumes of water. At this point, water and some residual oil remain in the porous medium. We now use one more syringe pump to inject the oil into the porous medium that flows simultaneously with the water at a total injection rate of 1 ml/min. We use different oil and water injection rates, q_o and q_w, respectively, to change and maintain a steady state saturation of the fluids in the porous medium. We start to inject oil at a flow rate of 0.25 ml/min and water at a flow rate of 0.75 ml/min until reaching a steady state. We confirm the steady state; when the

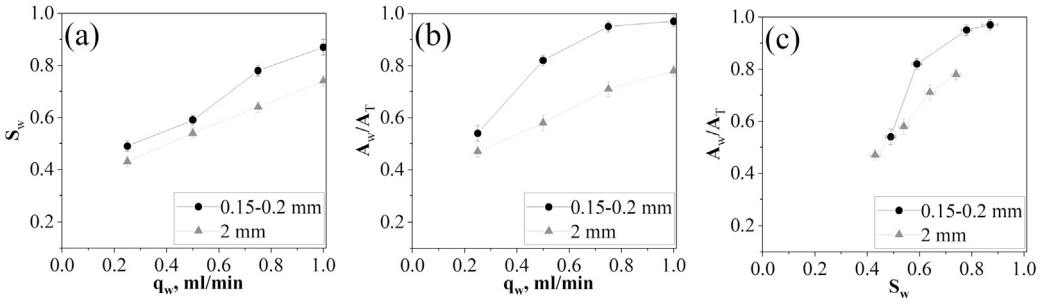

Fig. 3. The effect of grain size on (a) water saturation, (b) the fractional water-solid contact area; at different water injection rates, and (c) the fractional water-solid contact area as a function of the water saturation at different water injection rates, when water and oil flow simultaneously into the porous medium.

Table 3
Estimated K_a from the single-phase flow experiments (V = 47.10 ml).

Experiment	Q, $\frac{ml}{min}$	ϕ	$\tau_i = \phi V/Q$	A_T, g	$\tau_i = \int_0^\infty [1 - \frac{C_{exit}(t)}{C_T}]dt$, min (FSS)	$\tau_a = \int_0^\infty [1 - \frac{C_{exit}(t)}{C_T}]dt$, min (STS)	$(\tau_a - \tau_i)\frac{Q}{A_T} = K_a$, $\frac{ml}{g}$
HTE	1.00	0.42	19.78	78.87	19.67 ± 0.22	22.23 ± 0.31	**0.032**
	0.50	0.42	39.56	79.01	38.98 ± 0.31	44.13 ± 0.27	**0.033**
	0.25	0.42	79.13	78.98	80.01 ± 0.24	89.66 ± 0.28	**0.031**
VTE	1.00	0.42	19.78	78.87	20.03 ± 0.31	22.59 ± 0.32	**0.032**
	0.50	0.42	39.56	79.01	39.16 ± 0.29	44.21 ± 0.27	**0.032**
	0.25	0.42	79.13	78.98	81.11 ± 0.26	91.12 ± 0.28	**0.032**

exit stream has 75% water and 25% oil. At the steady state, we start to perform water-tracer flow experiments. After repeating the three sets of experiments at the same conditions, we increase the oil injection rate to 0.5 ml/min and decrease the water injection rate to 0.5 ml/min. Once it reaches a steady state, we similarly start water-tracer flow experiments as performed previously. After repeating the three sets of the tracer experiments at the same conditions, we increase the oil injection rate to 0.75 ml/min and decrease the water injection rate to 0.25 ml/min. Once it reaches a steady state, we start water-tracer flow experiments.

In Fig. 3 (a) and (b), we show the water saturation and the fractional water-solid contact area at different water injection rates, respectively, when water and oil flow simultaneously into the system. From Fig. 3 (a) and (b), we obtain that water saturation and water-solid contact area increases by increasing the water injection rates. The increase in the 2 mm beads pack is linear, while for the 0.2 mm beads pack, we see that the saturation and the water-solid contact area plateau near the higher flow rates. When we plotted the water-solid contact area vs the water saturation measured at various water injection rates, we noticed a similar relationship (see Fig. 3 (c)). Fig. 3 (c) also shows the plateauing of the solid-water contact area with water saturation obtained at different water injection rates when both phases flow in the porous medium. From these results, we obtained that larger beads show a linear relationship between the saturation, the water-solid contact area, and the flow rate. However, smaller beads show a non-linear relationship between the saturation, the water-solid contact area, and the flow rate (Singh et al., 2021, 2022). The cooperative pore-filling phenomenon (Zhao et al., 2016) causes this, in which a new, stable meniscus forms when two or more nearby meniscus overlap as the water flow rate rises in the system. The smaller beads have smaller pores; therefore, water imbibition is easier in smaller beads than the larger beads. Consequently, we reach the higher saturation and the water-solid contact area at lower flow rates in the smaller bead-sized porous medium and then obtain a plateau at higher flow rates.

3.2. Effect of gravity on measured water-solid contact area

In a porous medium, immiscible displacement of fluid flow regimes is affected by gravity in addition to the viscous and capillary forces. Therefore, we now analyse the impact of gravity on the water-solid contact area at different wetting phase saturations by varying water flow rates.

We use cleaned glass beads of diameters 2 mm to create a proxy porous medium. In the packed porous medium, we inject nine pore volumes of water at 1 ml/min from the bottom when the packing is oriented vertically. We prepare three separate water-saturated packings. We perform water-tracer flow experiments in all three packing at one given flow rate, i.e., 1 ml/min in packing 1, 0.5 ml/min in packing 2, and 0.25 ml/min in packing 3, as shown in Table 3. We first perform the water-tracer test when the packing is oriented horizontally and call them horizontal tracer experiments (HTE). We do the three repetitions of the test at one flow rate, say Q_i ml/min and then orient the packing vertically. In the vertically oriented packing, we inject water from the bottom and do the three water-tracer flow experiments in the packing at the same flow rate, i.e. Q_i ml/min and call vertical tracer experiments (VTE). Table 3 shows that the measured K_a of the adsorbing water-tracer in the packing is 0.03 ±0.002. From columns 4 and 6 of Table 3, we again see that the MRT calculated using process parameters and MRT from the tracer tests are similar, which validates our tracer tests. After completing the single-phase flow experiments in the vertical orientation, we flush out the tracers again by injecting several pore volumes of water. Once the tracer is flushed out, i.e. no tracer is seen under the UV-vis spectrum, we orient the packed tube horizontally again. Then we inject oil at a flow rate of 1 ml/min to reach the maximum oil saturation in all three packings. Once we achieve the steady state, i.e., the exit stream has only oil, we use the mass balance to get immobile water saturation of 0.25 ±0.01 in the packings. After that, we start to displace oil with water during the secondary imbibition process at the flow rate Q_i ml/min used in the previous experiments.

3.2.1. Estimation of water-solid contact area with residual oil saturation

Once we reach a steady state while displacing oil by injecting water at a flow rate Q_i ml/min while the packing is oriented horizontally (HTE), we follow the procedures described in Section 2.3 to perform the water tracer flow experiments. We calculate the MRTs using the exit concentration profile of the tracer at the residual oil saturation using Eqn. (3) and (4) for the ideal and the adsorbing tracers, respectively. We validate our experiments by comparing water saturation at this stage calculated (a) by material balance, Table 4 columns 5, and (b) using Eqns. (1) and (3), Table 4 columns 8. We use three repetitions of

Table 4
The estimated water-solid contact area (A_w) of the cleaned 2 mm glass beads at various residual oil saturation and different flow rates in different packing orientations (V = 47.10 ml).

Experiment	Flow rate (Q), $\frac{ml}{min}$	A_T, g	K_a,	S_w (MB)	τ_i' (FSS), min	τ_a' (STS), min	$S_w = \frac{\tau_a'}{\tau_i'}$	$A_w = (\tau_a' - \tau_i')\frac{Q}{K_a}$, g	$\frac{A_w}{A_T}$
HTE	1.00	78.87	0.032	0.83	15.93 ± 0.22	17.90 ± 0.24	0.81	61.56	0.78
	0.50	79.01	0.033	0.75	29.62 ± 0.26	33.12 ± 0.23	0.76	53.03	0.67
	0.25	78.98	0.031	0.69	54.41 ± 0.30	59.70 ± 0.27	0.68	42.66	0.54
VTE	1.00	78.87	0.032	0.84	17.03 ± 0.31	19.15 ± 0.27	0.85	66.25	0.84
	0.50	79.01	0.032	0.78	30.19 ± 0.25	33.87 ± 0.28	0.78	57.50	0.73
	0.25	78.98	0.032	0.73	57.59 ± 0.26	64.22 ± 0.29	0.71	51.80	0.66

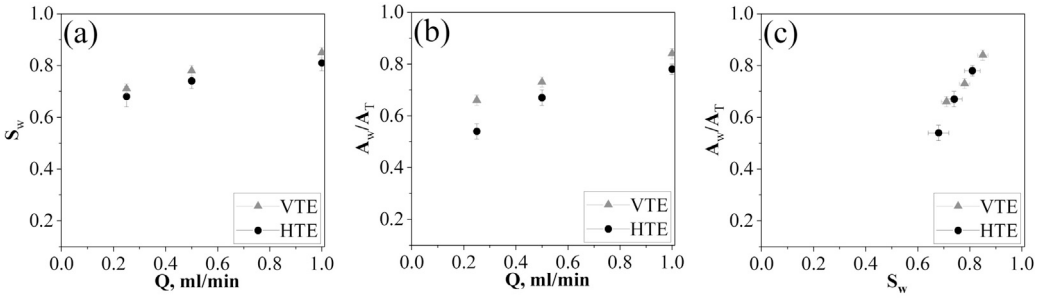

Fig. 4. Comparison of the HTE and VTE experimental results to analyse the relationship between (a) water saturation with the water injection rate (b) fraction of the glass beads surface area in contact with water (A_w/A_T) with the water injection rate, and (c) water-solid contact area vs saturation, when water is in the mobile phase, and oil is in the residual phase in the water-wet 2 mm sized glass bead packed system.

the water tracer experiments in the packing to calculate the water-solid contact area (A_w) using Eqns. (3) and (4) and show in column 9 of Table 4. After completing the two-phase flow experiment in the horizontal orientation, we flush out the tracers and do the same experiments in the vertical tube (VTE) at the same water injection rate from the bottom. As we change the orientation of the tube from horizontal to vertical, we obtain some more oil in the exit stream. Therefore, we calculate different residual oil saturation at the same water injection rate in the VTE in comparison to HTE. This is because of the density difference in oil and water (Brodin et al., 2022). In Fig. 4(a) and (b), we show the experimentally obtained water saturations and water-solid contact area at different water injection rates in HTE and VTE. In Fig. 4(c), we show the water saturation versus water-solid contact area for these cases. From this figure, we see that water saturation and A_w/A_T both linearly increase with an increase in water injection rate. We notice in the case where we inject water at a higher rate of 1 ml/min from the beginning, we see higher water saturation in comparison to Fig. 2. We also see that at low flow rates, gravity has a more pronounced effect on the water-solid contact area (Or et al., 2009). Therefore, in this case, saturation and water injection rate both affect the water-solid contact area.

3.2.2. Estimation of water-solid contact area with two flowing phases

Further, we use the setup used above at Q_i = 1 ml/min water injection rate to perform two-phase flow experiments. First, we perform water-tracer flow experiments in the horizontal orientation and then orient the tube vertically to perform the water-tracer flow experiments in identical conditions in the same packing. We use one more syringe pump to inject the oil into the porous medium. Using different oil and water injection rates q_o and q_w, respectively, we maintain a total injection rate of 1 ml/min into the porous system. The previous experiment ended when adsorbing water tracer was being injected at a flow rate of 1 ml/min in a VTE. First, we remove the adsorbing water tracer from the packing by injecting several pore volumes of water into the VTE. Then we orient the tube horizontally and inject oil at a flow rate of 0.25 ml/min and water at a flow rate of 0.75 ml/min till we reach a steady state. When the exit stream has 75% water and 25% oil, i.e., at the steady state, we start to perform the water-tracer flow experiments in the HTE. After repeating the three sets of experiments at the same conditions in the HTE, then we orient the tube vertically. First, we remove the adsorbing water tracer from the packing by injecting several pore volumes of water at a water flow rate of 0.75 ml/min while oil is flowing at a flow rate of 0.25 ml/min. We follow the same procedure as followed in HTE and perform water-tracer flow experiments in VTE. After repeating the three sets of experiments at the same conditions in the VTE, again, we keep the tube horizontal. We then remove the adsorbing water tracer from the packing by injecting water at a flow rate of 0.75 ml/min while oil is flowing at a flow rate of 0.25 ml/min. Now, we increase the oil injection rate to 0.5 ml/min and decrease the water injection rate to 0.5 ml/min. We do the tracer experiments in the horizontal tube and then in the vertical tube at the above flow rates. Once the tracer experiments in the VTE are completed for the water flow rate of 0.5 ml/min, then we orient the tube horizontally and flush out the tracers by injecting water at a flow rate of 0.5 ml/min while oil is flowing at a flow rate of 0.5 ml/min. We again decrease the water flow rate to 0.25 ml/min and increase the oil flow rate to 0.75 ml/min. At steady state, we start water-tracer flow experiments. We show the comparison of results for HTE and VTE in Fig. 5 (a), (b) and (c). In VTE, higher water saturations are observed at the same water flow rates. This is due to the buoyancy of oil leading to higher water saturation (Or et al., 2009). Due to the density difference, oil moves upward, and water movement increases the corner flow more in the vertical orientation. Due to that, we obtain more water-solid contact areas in VTE than the HTE at the same water injection rate. We see a linear relationship between water saturation and water injection rate, and water-solid contact area during the two-phase flow together in the porous medium.

3.3. Discussion for 2 mm glass beads experiments

In Fig. 6, we compare the flow experimental results obtained from 2 mm sized glass beads packing in different orientations; sequential and individual flow conditions when water is in the flowing phase, and the oil is in the residual phase in the system. From this figure, we show that (a) saturation changes are more pronounced due to injection rate when

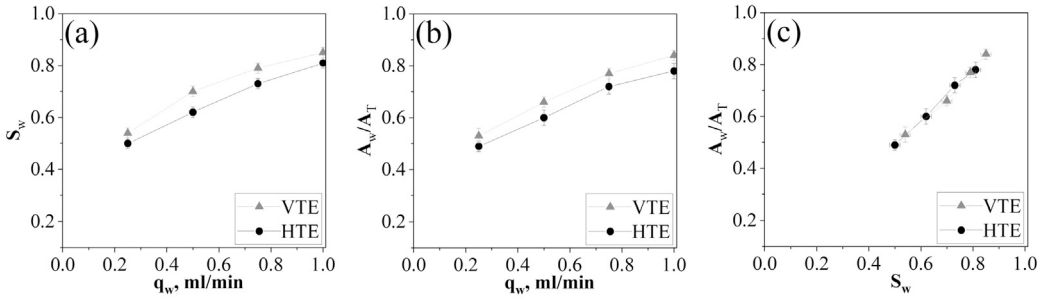

Fig. 5. Comparison of the HTE and VTE experimental results to analyse the relationship between (a) water saturation with the water injection rate (b) fraction of the glass beads surface area in contact with water (A_w/A_T) with the water injection rate, and (c) water-solid contact area vs saturation when oil and water both flowing simultaneously in the water-wet 2 mm sized glass bead packing.

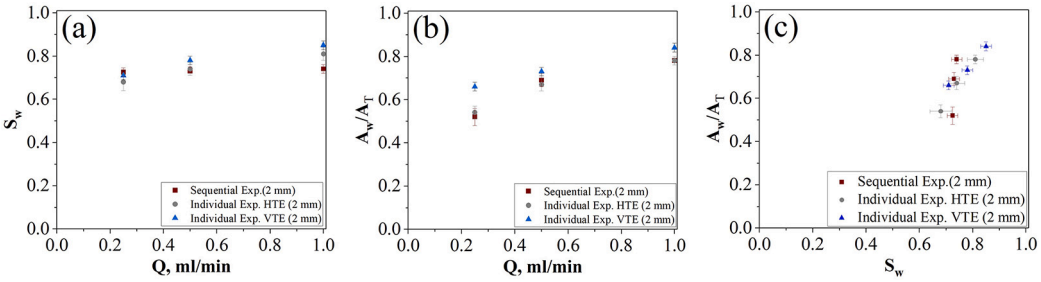

Fig. 6. Comparison of the flow experimental results when the only water flow in the glass beads packing at different oil saturation to analyse the relationship between the water injection rate with (a) water saturations S_w and (b) fractional solid-water interfacial area (A_w/A_T) and (c) A_w/A_T vs S_w.

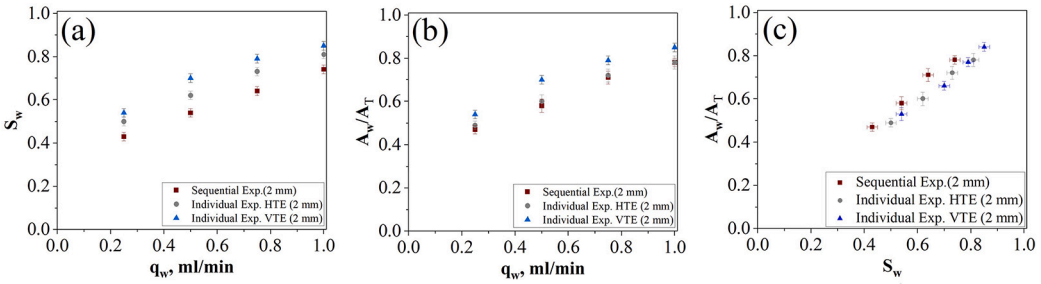

Fig. 7. Comparison of the two-phase flow experimental results when oil and water flow together in the glass beads packing to analyse the relationship between the water injection rate with (a) water saturation (S_w) (b) fraction of the glass bead surface area in contact with water (A_w/A_T) and (c) A_w/A_T vs S_w.

experiments are done directly at higher water injection rates rather than individually, and (b) gravity has a more pronounced effect on the water-solid contact area at a low flow rate. Therefore, the slope of the A_w/A_T vs S_w is dependent and affected by the flow process and presence and absence of gravity.

In Fig. 7, we show water saturations and water-solid interfacial areas at different water injection rates when water and oil flow simultaneously in the 2 mm sized glass bead packing. The combined results indicate the similarity of the relationship between water flow rate, water saturation and the solid-water interfacial area during the two-phase flow in the porous medium at different flow conditions. We see that the flow process, sequential and individual water injection, does not alter the water-solid contact area at different flow rates even though the saturation is different. From this, we can conclude that the increase in saturation is in the pore body primarily. While the contact area change in VTE and HTE curves is primarily driven by the change in saturation, we get the same slope of A_w/A_T vs S_w curve. This points to corner flow in VTE when the orientation changes from HTE. This result is consistent with the results of the prior study for liquid-liquid systems using the IPTT method in 1.16 mm glass beads packing (Zhong et al., 2016).

3.4. Effect of the surface morphology on measured water-solid contact area

After the implication of the tracer test in a smooth and controlled surface porous media, i.e., glass beads, we move toward the natural porous medium. Now, we analyse the effect of the surface morphology on the measured water-solid interfacial area.

We use the quartz sand (average grain diameter 200 μm similar to the smaller glass beads size in the above section) in its original state, purchased from GLR innovators in New Delhi, India. First, we analyse the surface morphology and composition of the glass beads and sand through scanning electron microscope (SEM) and X-Ray Diffraction (XRD) analyses. Fig. 8 shows that glass beads and sand have different surface morphology and compositions. Therefore, we investigate the presented method to directly quantify the wetted area of the solid by a liquid during the multiphase flow in a sand pack. We exactly follow the same procedure to perform single and two-phase flow experiments to estimate the water-solid interfacial area in the sand pack as discussed for glass beads in Section 3.1 by replacing glass beads with sand. First, we estimate the K_a of the adsorbing water tracer while the cylindrical packing orientation is horizontal using the methodology described in Section 2.3. Table 5 shows the results of single-phase flow experiments. The average estimated K_a using Eqns. (1) and (2) in the sand pack is 0.058 ± 0.0003 (ml/g).

Table 5
Estimated K_a for the adsorbing tracer (V = 47.10 ml).

Q, $\frac{ml}{min}$	ϕ	$\tau_i = \phi V/Q$, min	A_T, g	$\tau_i = \int_0^\infty [1 - \frac{C_{out}(t)}{C_T}]dt$, min (FSS)	$\tau_a = \int_0^\infty [1 - \frac{C_{out}(t)}{C_T}]dt$, min (STS)	$(\tau_a - \tau_i)\frac{Q}{A_T} = K_a$, $\frac{ml}{g}$
0.25	0.41	77.24	70.28	78.32 ± 0.36	94.76 ± 0.39	**0.058**
0.50	0.41	38.62	70.28	40.11 ± 0.46	48.23 ± 0.43	**0.058**
1.00	0.41	19.31	70.28	20.12 ± 0.42	24.17 ± 0.45	**0.058**

Table 6
The estimated water-solid contact area in the sand pack (A_w) at various residual oil saturation at different flow rates (V = 47.10 ml).

Flow rate (Q), $\frac{ml}{min}$	A_T, g	K_a, ml/gm	S_w (MB)	τ_i' (FSS), min	τ_a' (STS), min	$S_w = \frac{\tau_{ii}}{\tau_i}$	$A_w = (\tau_a' - \tau_i')\frac{Q}{K_a}$, g	$\frac{A_w}{A_T}$
0.25	70.28	0.058	0.89	71.27 ± 0.41	86.12 ± 0.38	0.91	63.96	0.91
0.50	70.28	0.058	0.90	36.58 ± 0.38	44.29 ± 0.36	0.91	66.47	0.95
1.00	70.28	0.058	0.90	18.43 ± 0.34	22.41 ± 0.36	0.92	68.62	0.98

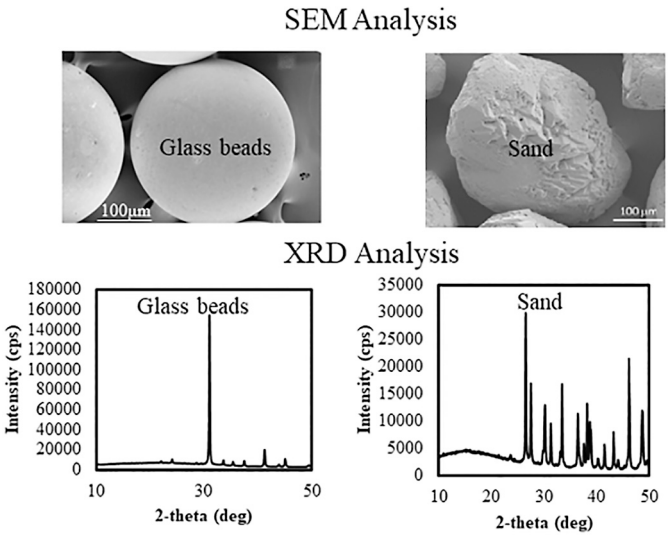

Fig. 8. The scanning electron microscope (SEM) and the X-Ray Diffraction (XRD) analyses at 10-50 degree diffraction; **Left** glass beads and **Right** sand.

3.4.1. Estimation of water-sand contact area in the sand pack at residual oil saturation

After completing the single-phase flow experiments, we inject oil at a flow rate of 1 ml/min to reach the maximum oil saturation. Once we reach a steady state, we use the mass balance and get immobile water saturation of 0.29 ± 0.01 in the sand pack. After that, we start to displace oil with water during the secondary imbibition process at a flow rate of 0.25 ml/min. Once we reach a steady state for the secondary imbibition and oil is immobile, i.e. at the residual saturation, the exit stream has only water. Then we follow the procedures described in Section 2.3 to perform the water tracer flow experiments. At this stage, we calculate the water saturation using Eqns. (1) and (3), and we compare it with the water saturation measured by the material balance. We show these results in Table 6 in columns 4 and 7 and see a good match in the saturations. We calculate the water-solid contact area (A_w) in the sand pack, while water is the mobile phase using Eqns. (3) and (4), and show in column 8 of Table 6. We use three repetitions of the water tracer experiments at the water flow rate of 0.25 ml/min. After that, we repeat the same water-tracer flow experiments at a water flow rate of 0.5 ml/min. We perform three sets of experiments at a 0.5 ml/min water flow rate and calculate the water-solid contact area (A_w) in the sand pack at this water injection rate. Sequentially we increase the water injection rate to 1 ml/min. We then complete three tracer experiments at a water injection rate of 1 ml/min and calculate the water-solid contact area (A_w) in the sand pack at this water injection rate and show in column 8 of Table 6. Hence, for consistency in all the experiments, we use the single sand pack, as we used single glass beads packing in Section 3.1. From the experimental results shown in Table 6, first, we find that water saturation does not change significantly with the increasing flow rate from 0.25 to 1 ml/min in the sand pack. However, the solid-water contact area increases with the increase in water injection rate. This observation is consistent with what we saw in the glass beads experiments in Section 3.1.2. Further, we compare the results of the 0.15-0.2 mm sized glass beads (from Fig. 2(b)) and sand (average grain diameter 0.2 mm) in Fig. 9(a) when water is mobile-phase, and oil is in the residual phase. From this figure, we observe higher water saturations and water-solid contact areas in the sand pack at the same water injection rates. This is due to the surface roughness of the sand (Jian-Chao et al., 2010), which affects the fluid behaviour by changing the degree of the wetting state and increasing the curvature of the interface (Jiang et al., 2020). Hence, it strengthens the capillary-driven flow at the corners leading to a more solid-water interfacial area in the sand pack than in glass beads.

3.4.2. Estimation of water-sand contact area in the sand pack with two flowing phases

In this case, we follow exactly the same procedure to perform two-phase flow experiments in the sand pack, as discussed for glass beads in Section 3.1.3. In this section, we compare the results of the two-phase flow experiments, when both phases flow simultaneously in the sand pack with the 0.15-0.2 mm sized glass beads, and show in Fig. 10(a) and 10(b). From Fig. 10(a), we observe higher water saturations in the sand pack than in the glass beads packing at the same water injection rates. This is due to the surface roughness. Further, from Fig. 10(b), we observe more water-solid contact area in a rough surface porous medium at the same flow rate. Figs. 10(b,c) show consistency in the observations for glass beads and sand particles of similar size. We see in smaller pores water imbibes in easily, therefore, we reach the higher saturation and contact area at lower flow rates due to the more corner flow in the smaller bead-sized porous medium and then see a plateau in the curve.

3.5. Effect of the flow process on measured water-solid contact area in the sand pack

Now, we move towards the different flow processes in the sand pack to analyse the water-solid contact area at various water injection rates and saturations. In this case, we use the same quartz sand which we used previously and conduct the water-tracer flow experiments in the two sand packs with liquid loading in two different ways, i.e., in one

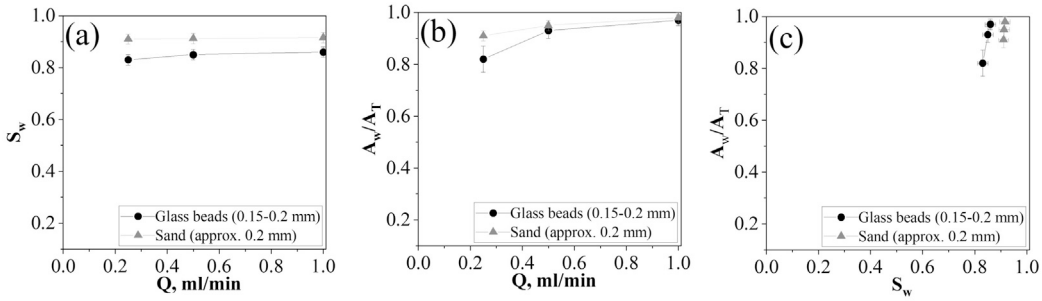

Fig. 9. Comparison of the two-phase flow experimental result performed in the sand pack with the same sized glass bead to analyse the relationship between the water injection rate with (a) water saturation (b) fraction of the sand surface area in contact with water (A_w/A_T), and (c) A_w/A_T vs S_w when water is mobile-phase, and oil is in residual-phase in the packings.

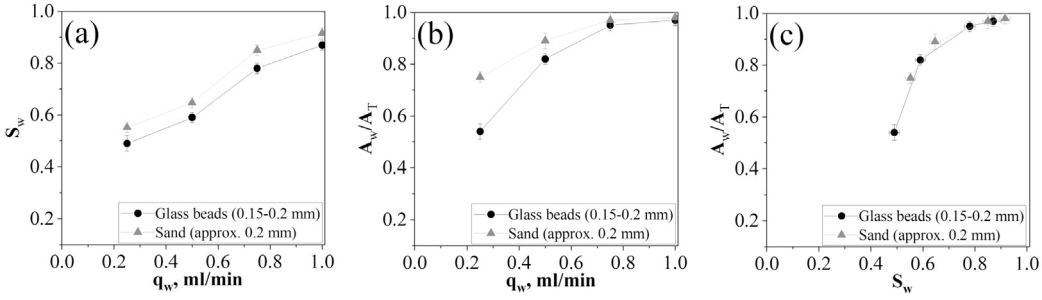

Fig. 10. Comparison of the two-phase flow experimental result performed in the sand pack with the same sized glass bead to analyse the relationship between the water injection rate with (a) water saturation (b) fraction of the sand surface area in contact with water (A_w/A_T), and (c) A_w/A_T vs S_w when oil and water flow simultaneously in the packings.

Table 7
Estimated K_a from the single-phase flow experiments in WF and OF (V = 47.10 ml).

Experiment	Q, $\frac{ml}{min}$	ϕ	$\tau_i = \phi V/Q$	A_T, g	$\tau_i = \int_0^\infty [1 - \frac{C_{exit}(t)}{C_T}]dt$, min (FSS)	$\tau_a = \int_0^\infty [1 - \frac{C_{exit}(t)}{C_T}]dt$, min (STS)	$(\tau_a - \tau_i)\frac{Q}{A_T} = K_a$, $\frac{ml}{g}$
WF	0.25	0.41	77.24	71.17	78.67 ± 0.35	95.18 ± 0.38	**0.058**
	0.50	0.41	38.62	71.17	40.32 ± 0.36	48.53 ± 0.34	**0.058**
	0.75	0.41	25.75	71.17	26.87 ± 0.31	32.36 ± 0.33	**0.058**
	1.00	0.41	19.31	71.17	20.54 ± 0.36	24.67 ± 0.32	**0.058**
Experiment	Q, $\frac{ml}{min}$	ϕ	$\tau_i = \phi V/Q$	A_T, g	$\tau_i = \int_0^\infty [1 - \frac{C_{exit}(t)}{C_T}]dt$, min (TSB)	$\tau_a = \int_0^\infty [1 - \frac{C_{exit}(t)}{C_T}]dt$, min (Oil Red O)	$(\tau_a - \tau_i)\frac{Q}{A_T} = K_a$, $\frac{ml}{g}$
OF	0.25	0.41	77.24	71.02	74.65 ± 0.28	111.58 ± 0.27	**0.13**
	0.50	0.41	38.62	71.02	36.45 ± 0.26	55.20 ± 0.26	**0.13**
	0.75	0.41	25.75	71.02	24.12 ± 0.21	36.71 ± 0.23	**0.13**
	1.00	0.41	19.31	71.02	18.78 ± 0.23	28.08 ± 0.27	**0.13**

sand pack, we load water first (calling the experiments WF), and in the second sand pack, we load oil first (calling the experiments OF). For the WF (water first) experiments, we first inject the water at a rate of 1 ml/min in the sand pack from the bottom while the tube is oriented vertically. We find the porosity of the water-saturated sand pack is 0.41 ± 0.02. We then perform the single-phase flow experiments, i.e., we perform the water-tracer flow experiments at flow rates 0.25, 0.5, 0.75 and 1 ml/min to estimate the K_a of the water tracer while the cylindrical packing orientation is horizontal using the methodology described in Section 2.3. For the OF (oil first) experiments, we first inject the oil at a rate of 1 ml/min in the sand pack from the bottom while the tube is oriented vertically. We find the porosity of the oil-saturated sand pack is 0.41 ± 0.01. We then perform the single-phase flow experiments, i.e., we perform the oil-tracer flow experiments at flow rates 0.25, 0.5, 0.75 and 1 ml/min to estimate the K_a of the oil tracer while the cylindrical packing orientation is horizontal using the methodology described in Section 2.3. The estimated K_a values from water-tracer and oil-tracer experiments are 0.058 ± 0.0003 and 0.13 ± 0.002 as shown in Table 7. We use this estimated K_a in the two-phase flow experiments for the corresponding water/oil-solid interfacial area measurement. The single-phase flow experiment ends with the adsorbing tracer. Therefore, first, we remove the adsorbing tracer from the WF and OF sand packs by injecting various pore volumes of water and oil, respectively. Now, the sand pack of the WF experiment is fully saturated with water, and OF is saturated with oil. Therefore, to reach the initial conditions in the WF sand pack, we inject oil at a 1 ml/min flow rate. Once we get a steady state, i.e., the exit stream has only oil, and the water is immobile, we measure the water saturation of 30 ± 1% in the WF experiment by the material balance. However, OF sand pack has 100% oil.

3.5.1. Estimation of water-solid contact area with residual oil saturation in WF and OF

At this point, we have 70 ± 1% oil saturation in WF and 100% oil saturation in OF. Now, We exactly follow the same procedure to perform the two-phase flow experiments and measure the water-solid contact area at different residual oil saturations at 0.25, 0.5, 0.75, and 1 ml/min in the WF and OF experiments as discussed for glass beads in Section 3.1. We report our measurements in Table 8. Due to the

Table 8
The estimated water-solid contact area (A_w) in the sand pack at various residual oil saturation and different flow rates (V = 47.10 ml).

Experiment	Flow rate (Q), $\frac{ml}{min}$	A_T, g	K_a,	S_w (MB)	τ_i' (FSS), min	τ_a' (STS), min	$S_w = \frac{\tau_i}{\tau_i}$	$A_w = (\tau_a' - \tau_i')\frac{Q}{K_a}$, g	$\frac{A_w}{A_T}$
WF	0.25	71.17	0.058	0.89	71.59 ± 0.28	86.62 ± 0.31	0.910	64.76	0.91
	0.50	71.17	0.058	0.90	36.73 ± 0.34	44.41 ± 0.30	0.911	66.19	0.93
	0.75	71.17	0.058	0.90	24.51 ± 0.35	29.73 ± 0.35	0.912	67.61	0.95
	1.00	71.17	0.058	0.90	18.81 ± 0.32	22.86 ± 0.33	0.916	69.75	0.98
OF	0.25	71.02	0.058	0.85	68.35 ± 0.29	81.86 ± 0.31	0.869	58.24	0.82
	0.50	71.02	0.058	0.86	35.05 ± 0.27	41.88 ± 0.32	0.869	58.95	0.83
	0.75	71.02	0.058	0.86	23.38 ± 0.28	28.05 ± 0.29	0.870	60.37	0.85
	1.00	71.02	0.058	0.86	17.89 ± 0.26	21.52 ± 0.30	0.871	62.50	0.88

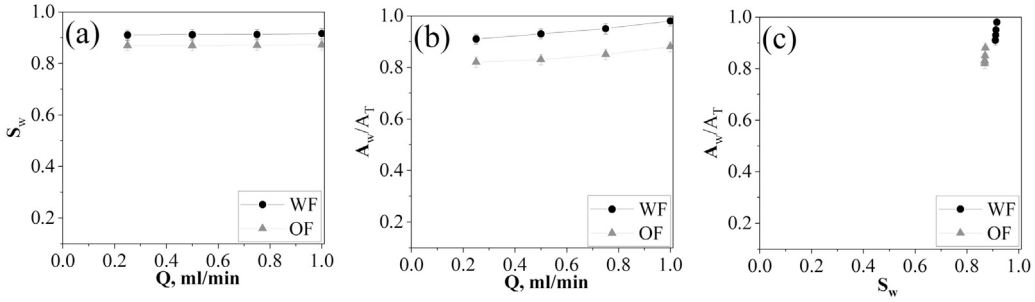

Fig. 11. Comparison of the two-phase flow experimental result performed in WF and OF to analyse the relationship between the water injection rate with (a) water saturation (b) fraction of the sand surface area in contact with water (A_w/A_T), and (c) A_w/A_T vs S_w when oil is in the residual-phase and water is only mobile in the sand pack.

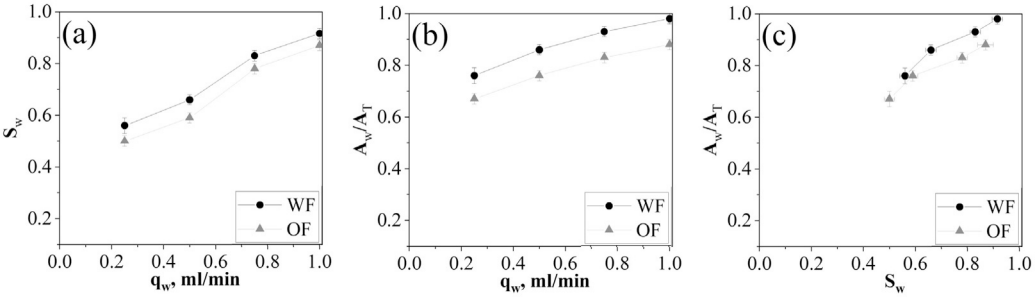

Fig. 12. Comparison of the two-phase flow experimental result performed in WF and OF to analyse the relationship between the water injection rate with (a) water saturation (b) fraction of the sand surface area in contact with water (A_w/A_T) and (c) A_w/A_T vs S_w when oil and water flow together in the sand pack.

capillary dominating effect, we do not recover a significant amount of extra oil from the sand pack when the flow rate increases from 0.25 to 1 ml/min as seen in Table 8. However, the water-solid contact area increases with the increase in water injection rate in WF and OF experiments. This observation is the same as what we saw in the glass beads experiments in Section 3.1.2. This is due to the corner flow phenomenon and surface roughness. From Table 8, we observe 4-4.5% higher residual oil in the OF experiment during the secondary imbibition process than in the WF experiments due to higher initial oil saturation in OF. In Fig. 11(a) and (b), we show the estimated water saturation and fractional water-solid interfacial area at different water injection rates during the two-phase flow experiments when water is in the mobile phase, and oil is in the residual phase. This result aligns with our expectations of having a more water-solid interfacial area in WF than in OF due to the more residual oil in OF packing. This figure also shows that wettability has a more prominent influence on the liquid-solid interfacial area, as seen from the flow rates compared to the saturations. Therefore, we obtained that flow conditions also significantly affect the interfacial area. In Fig. 11(c), we show the correspondingly calculated water saturation versus fractional water-solid interfacial area in WF and OF experiments. This result aligns with our expectations. This observation is the same as what we saw in the glass beads experiments in Section 3.1.2.

3.5.2. *Estimation of water-solid contact area when water and oil flow together in WF and OF experiments*

Further, we use the same setup to perform the two-phase flow experiments where water and oil flow simultaneously in WF and OF experiments. We follow the same procedure and the steps for the water-solid interfacial area measurements during the two-phase flow in the WF and OF experiments as we discussed in Section 3.1.3. In Fig. 12 (a), we show the water saturation at different water injection rates when water and oil flow simultaneously in the WF and OF sand pack. At the same water flow rate, we obtain more water saturation in WF than in OF due to the water flow from the pore surface boundaries being more in WF. These results align with our expectations as WF was initially saturated with water and OF with oil. In Fig. 12 (b), we show the fractional sand surface area in contact with water (A_w/A_T) at a range of water flow rates when water and oil flowed simultaneously in WF and OF. In this situation, we obtain that at the same water injection rate, we get a higher water-solid contact area in the WF experiment than in the OF experiments due to the different flow processes. From Fig. 12 (c), we obtain

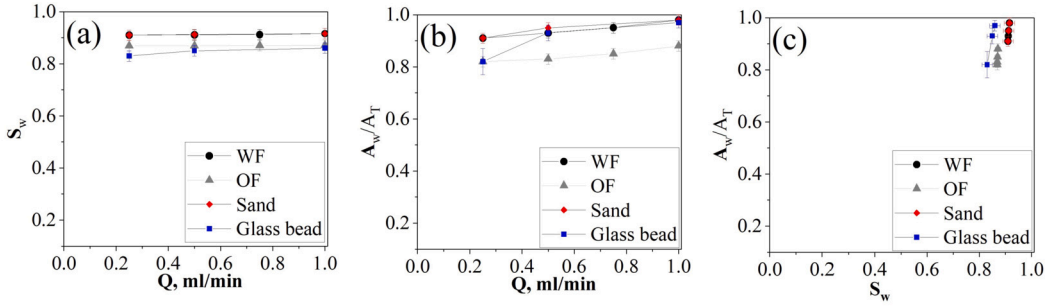

Fig. 13. Comparison of the two-phase flow experimental results when water flows at different flow rates in the porous medium at different residual oil saturations to analyse the relationship between the water injection rate with (a) water saturation (S_w) (b) fraction of the solid surface area in contact with water (A_w/A_T) and (c) A_w/A_T vs S_w when oil and water flow together in the porous medium.

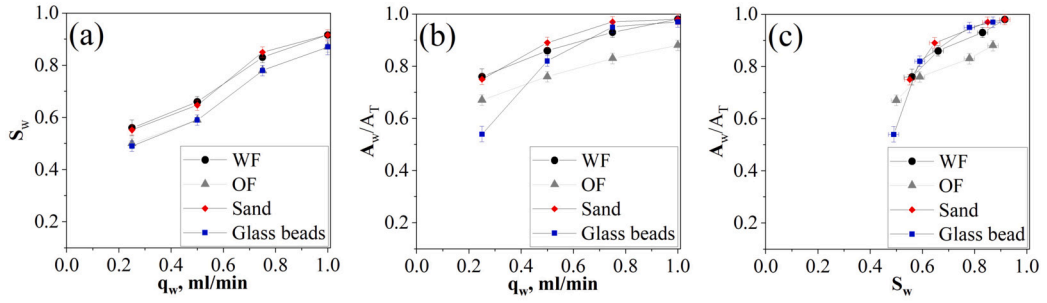

Fig. 14. Comparison of the two-phase flow experimental results when oil and water flow together in the porous medium to analyse the relationship between the water injection rate with (a) water saturation (S_w) (b) fraction of the solid surface area in contact with water (A_w/A_T) and (c) A_w/A_T vs S_w when oil and water flow together in the porous medium.

a monotonic increasing non-linear relationship between water saturation and water-solid contact area when oil and water flow together in a porous medium. This analysis shows that different flow processes to reach saturation affect the water-solid contact area.

3.5.3. Discussion for sand experiments

In Fig. 13, we compare the flow experimental results obtained from WF and OF with the sand and smaller beads size glass beads when water is the flowing phase and oil is the residual phase. From this figure, we show that there is a significant change in the water-solid contact area with flow rates. However, there is no significant change in saturation at different water injection rates. This means that the flow rate governs the corner flow and hence the water-solid contact area, and this is consistent with our observation in 2 mm glass beads as well.

In Fig. 14, we show a complete set of flow experimental results when water and oil flow simultaneously in the porous medium. The combined results indicate the similarity in the relationship between the flow rate and the water saturation and the flow rate and the solid-water interfacial area. We obtain a concave relationship between solid-water interfacial area and saturation at different flow rates during multiphase flow in a natural and smaller bead-size porous medium. As discussed earlier, this is due to dominating corner flow in small pores.

3.6. Validation of the measured water-solid contact area in the natural porous medium

We now show a few results from our experiments to validate the measured water-solid interfacial area in the natural porous medium, i.e., sand. In this case, after completing the two-phase flow experiments at the water flow rate of 0.25 ml/min and the oil flow rate of 0.75 ml/min. We use the same setup and inject the water and oil simultaneously at the flow rates of 0.5 ml/min individually. We maintained a steady state at a flow rate of 0.5 ml/min for both the phases in the WF and OF experiments, i.e., at the exit, we produced water at a flow rate of 0.5 ml/min and oil at a rate of 0.5 ml/min. Now at this point, we first inject the ideal tracer of both phases and calculate the MRT of the ideal tracer by the tracer concentration profile. After that, we flush the tracer by injecting several pore volumes of water and oil. Next, we inject adsorbing tracers of oil and water together at a flow rate of 0.5 ml/min and use Eqns. (3) and (4), and corresponding the K_a from Table 7, we calculate water-solid (A_w) and oil-solid (A_o) contact areas independently using tracers' exit age density curves, as given in Table 9. After calculations, we obtained $A_w/A_T + A_o/A_T = 1$, which validates our methodology that our measurements give liquid-solid interfacial area during the multiphase flow in a porous system.

4. Discussion on wettability and liquid-solid contact area

In our experiments, we quantified the liquid-solid contact area for different saturation and flow conditions. In addition, we show how the grain size, gravity, and surface heterogeneity in the case of sand and flow process affect the liquid-solid contact area. To quantify wettability, we need to establish a correspondence between the measured liquid-solid contact area with other established methods of quantifying wettability. The most popular method is using a contact angle. Fig. 15 (a) shows a schematic of two drops of the same volume that have different contact angles with a surface. We can see that the liquid-solid contact area will change if the contact angle changes, given the volume of the drops is kept the same. Fig. 15 (b) shows how the normalised contact area, calculated geometrically, changes with the contact angle for a given volume of the drop. Therefore, when we quantify the liquid-solid contact area, we need to relate it with the liquid volume in the porous medium or need to find a representation of the liquid-solid contact area per unit volume of the porous medium to relate it with saturation. In our experiments, because the porosity and porous medium do not change significantly, therefore, saturation is a representation of the volume. However, in real systems, we need to consider the volume and the liquid saturation separately for wettability quantification.

In addition to the parameters shown in our work, we need to understand how the porosity, particle shape, particle size distribution and

Table 9
Estimation of the fraction of liquid-solid interfacial area when oil and water are simultaneously flowing through the porous medium at different flow processes ($V = 47.10$ ml).

Experiment	q_w, $\frac{ml}{min}$	K_a, $\frac{ml}{g}$	ϕ	τ_{ii} (FSS), min	τ_{aa} (STS), min	$A_w = (\tau_{aa} - \tau_{ii})\frac{q_w}{K_a}$, g	A_T	$\frac{A_w}{A_T}$
WF	0.50	0.058	0.41	26.61	33.73	61.36	71.17	0.86
Experiment	q_o, $\frac{ml}{min}$	K_a, $\frac{ml}{g}$	ϕ	τ_{ii} (TSB), min	τ_{aa} (Oil-Red), min	$A_o = (\tau_{aa} - \tau_{ii})\frac{q_o}{K_a}$, g	A_T	$\frac{A_0}{A_T}$
WF	0.50	0.13	0.41	24.12	26.71	9.96	71.17	0.14
Experiment	q_w, $\frac{ml}{min}$	K_a, $\frac{ml}{g}$	ϕ	τ_{ii} (FSS), min	τ_{aa} (STS), min	$A_w = (\tau_{aa} - \tau_{ii})\frac{q_w}{K_a}$, g	A_T	$\frac{A_w}{A_T}$
OF	0.50	0.058	0.41	22.23	28.49	53.90	71.02	0.76
Experiment	q_o, $\frac{ml}{min}$	K_a, $\frac{ml}{g}$	ϕ	τ_{ii} (TSB), min	τ_{aa} (Oil-Red), min	$A_o = (\tau_{aa} - \tau_{ii})\frac{q_o}{K_a}$, g	A_T	$\frac{A_0}{A_T}$
OF	0.50	0.13	0.41	20.12	24.64	17.38	71.02	0.24

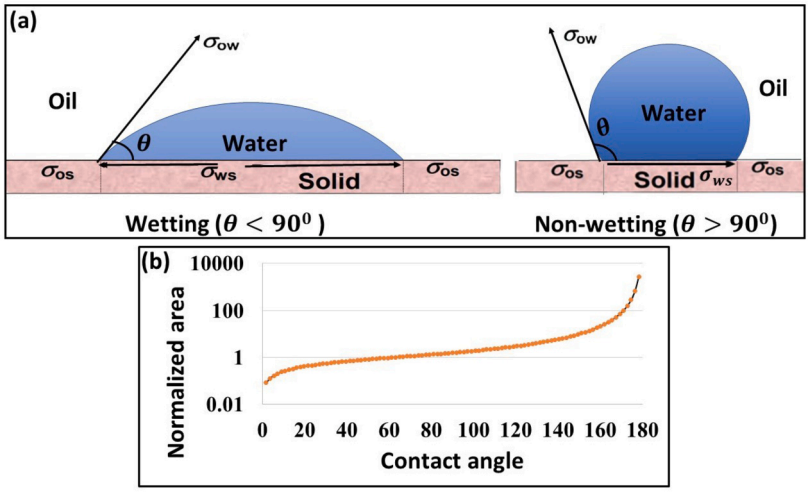

Fig. 15. (a) Behaviour of the wetting versus non-wetting liquid/solid surface. Here we show the surface interactions between three phases (solid-water-oil) when the same volume of liquid is in contact with wetting and non-wetting surface. Here, θ is the angle measured through the water phase, where a water-oil interface meets on the solid surface, σ_{ws} is the interfacial tension between the solid and water phase, σ_{os} is the interfacial tension between the solid and oil phase, and σ_{ow} is the interfacial tension between the water and oil phase, (b) behaviour of the solid-liquid contact area with the contact angle for a given volume of the drop.

surface chemical compositions will affect the liquid-solid contact area to derive a constitutive relation between wettability and liquid-solid contact area.

5. Summary and conclusions

We have systematically explored the two-tracer technique, performed a series of flow experiments with the ideal and adsorbing tracers and measured the liquid-solid interfacial area during the multiphase flow in the different packings, flow conditions, saturations and flow processes.

We have shown that different parameters, i.e., grain size, gravity, surface morphology, flow conditions, saturation and flow process to reach saturation, affect the measured water-solid interfacial area during the multiphase flow in the porous medium. We performed experiments in two ways (a) when oil is residual and water is flowing (b) when both phases are flowing. When only water is in the flowing phase, we saw that the flow rate does not affect the saturation significantly while increasing the corner flow, and hence the water-solid contact area increases with an increase in the water injection rate. When both oil and water are flowing, the saturation in the porous medium changes by the design of experiments. We see a linear relationship in the water-solid contact area with water saturation for larger pores and a concave downward, increasing curve of the water-solid contact area with water saturation for smaller pores. This is due to the corner flow and cooperative filling phenomenon in the smaller bead-sized glass beads and sand packing when oil and water flow together in the porous medium.

These results can be further used to develop a relationship between different parameters and water-solid contact area that can be used as a proxy for wettability in large porous media.

Declaration of competing interest

The authors declare that they have no known competing financial interests or personal relationships that could have appeared to influence the work reported in this paper.

Data availability

No data was used for the research described in the article.

Acknowledgement

The authors thank the Board of Research in Nuclear Sciences, Department of Atomic Energy, India, for financial support, project number: 35/14/50/2014-BRNS.

Appendix A. Supplementary material

Supplementary material related to this article can be found online at https://doi.org/10.1016/j.ces.2023.118992.

References

Akyazi, T., Basabe-Desmonts, L., Benito-Lopez, F., 2018. Review on microfluidic paper-based analytical devices towards commercialisation. Anal. Chim. Acta 1001, 1–17.

Alhosani, A., Bijeljic, B., Blunt, M.J., 2021. Pore-scale imaging and analysis of wettability order, trapping and displacement in three-phase flow in porous media with various wettabilities. Transp. Porous Media 140 (1), 59–84.

Anderson, W., 1986b. Wettability literature survey-Part 2: Wettability measurement. J. Pet. Technol. 38 (11), 1246–1262.

Anderson, W.G., 1986a. Wettability literature survey-Part 1: Rock/oil/brine interactions and the effects of core handling on wettability. J. Pet. Technol. 38 (10), 1125–1144.

Anderson, W.G., 1986c. Wettability literature survey-Part 3: The effects of wettability on the electrical properties of porous media. J. Pet. Technol. 38 (12), 1371–1378.

Anderson, W.G., 1987a. Wettability literature survey-Part 4: Effects of wettability on capillary pressure. J. Pet. Technol. 39 (10), 1283–1300.

Anderson, W.G., 1987b. Wettability literature survey-Part 5: The effects of wettability on relative permeability. J. Pet. Technol. 39 (11), 1453–1468.

Anderson, W.G., 1987c. Wettability literature survey-Part 6: The effects of wettability on waterflooding. J. Pet. Technol. 39 (12), 1605–1622.

Araújo, J.B., Brusseau, M.L., 2019. Novel fluid–fluid interface domains in geologic media. Environ. Sci. Process. Impacts 21 (1), 145–154.

Armstrong, R.T., McClure, J.E., Berrill, M.A., Rücker, M., Schlüter, S., Berg, S., 2016. Beyond Darcy's law: the role of phase topology and ganglion dynamics for two-fluid flow. Phys. Rev. E 94 (4), 043113.

Armstrong, R.T., McClure, J.E., Robins, V., Liu, Z., Arns, C.H., Schlüter, S., Berg, S., 2019. Porous media characterization using Minkowski functionals: theories, applications and future directions. Transp. Porous Media 130, 305–335.

Armstrong, R.T., Sun, C., Mostaghimi, P., Berg, S., Rücker, M., Luckham, P., Georgiadis, A., McClure, J.E., 2021. Multiscale characterization of wettability in porous media. Transp. Porous Media 140 (1), 215–240.

Ashraf, S., Méheust, Y., Phirani, J., 2023. Spontaneous imbibition dynamics in two-dimensional porous media: a generalized interacting multi-capillary model. Phys. Fluids 35 (1), 012005.

Brodin, J.F., Rikvold, P.A., Moura, M., Toussaint, R., Måløy, K.J., 2022. Competing gravitational and viscous effects in 3d two-phase flow investigated with a table-top optical scanner. Front. Phys., 596.

Brusseau, M.L., Peng, S., Schnaar, G., Murao, A., 2007. Measuring air- water interfacial areas with x-ray microtomography and interfacial partitioning tracer tests. Environ. Sci. Technol. 41 (6), 1956–1961.

Brusseau, M.L., Narter, M., Schnaar, G., Marble, J., 2009. Measurement and estimation of organic-liquid/water interfacial areas for several natural porous media. Environ. Sci. Technol. 43 (10), 3619–3625.

Brusseau, M.L., Narter, M., Janousek, H., 2010. Interfacial partitioning tracer test measurements of organic-liquid/water interfacial areas: application to soils and the influence of surface roughness. Environ. Sci. Technol. 44 (19), 7596–7600.

Cai, J., Yu, B., 2010. Prediction of maximum pore size of porous media based on fractal geometry. Fractals 18 (04), 417–423.

Cense, A., Berg, S., 2009. The viscous-capillary paradox in 2-phase flow in porous media. In: International Symposium of the Society of Core Analysts Held in Noordwijk, the Netherlands, pp. 27–30.

Chen, Y., Xie, Q., Sari, A., Brady, P.V., Saeedi, A., 2018. Oil/water/rock wettability: influencing factors and implications for low salinity water flooding in carbonate reservoirs. Fuel 215, 171–177.

Christensen, M., Tanino, Y., 2017. Waterflood oil recovery from mixed-wet limestone: dependence upon the contact angle. Energy Fuels 31 (2), 1529–1535.

Farokhpoor, R., Bjørkvik, B.J., Lindeberg, E., Torsæter, O., 2013. CO_2 wettability behavior during CO_2 sequestration in saline aquifer-an experimental study on minerals representing sandstone and carbonate. Energy Proc. 37, 5339–5351.

Garfi, G., John, C.M., Lin, Q., Berg, S., Krevor, S., 2020. Fluid surface coverage showing the controls of rock mineralogy on the wetting state. Geophys. Res. Lett. 47 (8), e2019GL086380.

Golparvar, A., Zhou, Y., Wu, K., Ma, J., Yu, Z., 2018. A comprehensive review of pore scale modeling methodologies for multiphase flow in porous media. Adv. Geo-Energy Res. 2 (4), 418–440.

Günther, A., Jensen, K.F., 2006. Multiphase microfluidics: from flow characteristics to chemical and materials synthesis. Lab Chip 6 (12), 1487–1503.

Herring, A., Sun, C., Armstrong, R., Li, Z., McClure, J., Saadatfar, M., 2021. Evolution of Bentheimer sandstone wettability during cyclic scco2-brine injections. Water Resour. Res. 57 (11), e2021WR030891.

Huling, S.G., Weaver, J.W., 1991. Dense nonaqueous phase liquids. Superfund Technology Support Center for, Ground Water and Kerr, Robert S.

Jain, V., Bryant, S., Sharma, M., 2003. Influence of wettability and saturation on liquid-liquid interfacial area in porous media. Environ. Sci. Technol. 37 (3), 584–591.

Jeon, D.H., 2019. Wettability in electrodes and its impact on the performance of lithium-ion batteries. Energy Storage Mater. 18, 139–147.

Jian-Chao, C., Bo-Ming, Y., Ming-Qing, Z., Mao-Fei, M., 2010. Fractal analysis of surface roughness of particles in porous media. Chin. Phys. Lett. 27 (2), 024705.

Jiang, H., Guo, B., Brusseau, M.L., 2020. Pore-scale modeling of fluid-fluid interfacial area in variably saturated porous media containing microscale surface roughness. Water Resour. Res. 56 (1), e2019WR025876.

Joekar-Niasar, V., Hassanizadeh, S., 2012. Analysis of fundamentals of two-phase flow in porous media using dynamic pore-network models: a review. Crit. Rev. Environ. Sci. Technol. 42 (18), 1895–1976.

Joekar-Niasar, V., Hassanizadeh, S., Leijnse, A., 2008. Insights into the relationships among capillary pressure, saturation, interfacial area and relative permeability using pore-network modeling. Transp. Porous Media 74 (2), 201–219.

Ju, B., Fan, T., Li, Z., 2012. Improving water injectivity and enhancing oil recovery by wettability control using nanopowders. J. Pet. Sci. Eng. 86, 206–216.

Li, J., Hong, F., Xie, R., Cheng, P., 2019. Pore scale simulation of evaporation in a porous Wick of a loop heat pipe flat evaporator using lattice Boltzmann method. Int. Commun. Heat Mass Transf. 102, 22–33.

Lin, Q., Bijeljic, B., Berg, S., Pini, R., Blunt, M.J., Krevor, S., 2019. Minimal surfaces in porous media: pore-scale imaging of multiphase flow in an altered-wettability Bentheimer sandstone. Phys. Rev. E 99 (6), 063105.

Liu, Z., Herring, A., Arns, C., Berg, S., Armstrong, R.T., 2017. Pore-scale characterization of two-phase flow using integral geometry. Transp. Porous Media 118 (1), 99–117.

McClure, J.E., Berrill, M.A., Gray, W.G., Miller, C.T., 2016. Influence of phase connectivity on the relationship among capillary pressure, fluid saturation, and interfacial area in two-fluid-phase porous medium systems. Phys. Rev. E 94 (3), 033102.

McClure, J.E., Armstrong, R.T., Berrill, M.A., Schlüter, S., Berg, S., Gray, W.G., Miller, C.T., 2018. Geometric state function for two-fluid flow in porous media. Phys. Rev. Fluids 3 (8), 084306.

Nemec, P., 2017. Porous structures in heat pipes. In: Porosity-Process, Technologies and Applications.

Or, D., Tuller, M., Jones, S.B., 2009. Liquid behavior in partially saturated porous media under variable gravity. Soil Sci. Soc. Am. J. 73 (2), 341–350.

Rücker, M., Bartels, W.-B., Garfi, G., Shams, M., Bultreys, T., Boone, M., Pieterse, S., Maitland, G., Krevor, S., Cnudde, V., et al., 2020. Relationship between wetting and capillary pressure in a crude oil/brine/rock system: from nano-scale to core-scale. J. Colloid Interface Sci. 562, 159–169.

Russo, A., Narter, M., Brusseau, M., 2009. Characterizing pore-scale dissolution of organic immiscible liquid in a poorly-sorted natural porous medium. Environ. Sci. Technol. 43 (15), 5671–5678.

Schnaar, G., Brusseau, M., 2005. Pore-scale characterization of organic immiscible-liquid morphology in natural porous media using synchrotron x-ray microtomography. Environ. Sci. Technol. 39 (21), 8403–8410.

Schwartz, J., Weger, E., Duduković, M., 1976. A new tracer method for determination of liquid-solid contacting efficiency in trickle-bed reactors. AIChE J. 22 (5), 894–904.

Singh, D., Roy, S., Pant, H.J., Phirani, J., 2021. Solid-fluid interfacial area measurement for wettability quantification in multiphase flow through porous media. Chem. Eng. Sci. 231, 116250.

Singh, D., Roy, S., Pant, H.J., Phirani, J., 2022. A novel approach for wettability estimation in geological systems by fluid-solid interfacial area measurement using tracers. J. Pet. Sci. Eng., 110722.

Singhal, A., Dranchuk, P., 1975. Wettability control of glass beads. Can. J. Chem. Eng. 53 (1), 3–8.

Standnes, D.C., Austad, T., 2000. Wettability alteration in chalk: 2. Mechanism for wettability alteration from oil-wet to water-wet using surfactants. J. Pet. Sci. Eng. 28 (3), 123–143.

Standnes, D.C., Austad, T., 2003. Wettability alteration in carbonates: interaction between cationic surfactant and carboxylates as a key factor in wettability alteration from oil-wet to water-wet conditions. Colloids Surf. A, Physicochem. Eng. Asp. 216 (1–3), 243–259.

Strand, S., Standnes, D., Austad, T., 2006. New wettability test for chalk based on chromatographic separation of SCN^- and $SO4^{2-}$. J. Pet. Sci. Eng. 52 (1–4), 187–197.

Tabar, M.A., Ghazanfari, M.H., Monfared, A.D., 2020. Compare numerical modeling and improved understanding of dynamic sessile drop contact angle analysis in liquid-solid-gas system. J. Pet. Sci. Eng. 184, 106552.

Tian, D., Song, Y., Jiang, L., 2013. Patterning of controllable surface wettability for printing techniques. Chem. Soc. Rev. 42 (12), 5184–5209.

Woudt, B.D.v., 1959. Particle coatings affecting the wettability of soils. J. Geophys. Res. 64 (2), 263–267.

Yao, M., Tijing, L.D., Naidu, G., Kim, S.-H., Matsuyama, H., Fane, A.G., Shon, H.K., 2020. A review of membrane wettability for the treatment of saline water deploying membrane distillation. Desalination 479, 114312.

Zhao, B., MacMinn, C.W., Juanes, R., 2016. Wettability control on multiphase flow in patterned microfluidics. Proc. Natl. Acad. Sci. 113 (37), 10251–10256.

Zhong, H., El Ouni, A., Lin, D., Wang, B., Brusseau, M.L., 2016. The two-phase flow IPTT method for measurement of nonwetting-wetting liquid interfacial areas at higher non-wetting saturations in natural porous media. Water Resour. Res. 52 (7), 5506–5515.